Materials Transactions, Vol. 56, No. 3 (2015) pp. 372 to 376

Production of Nanocrystalline (Fe, Co)-Si-B-P-Cu Alloy with Excellent Soft Magnetic Properties for Commercial Applications

Kana Takenaka[1,*], Albertus D. Setyawan[1], Yan Zhang[2], Parmanand Sharma[1], Nobuyuki Nishiyama[1] and Akihiro Makino[1,2]

[1]*Research and Development Center for Ultra High Efficiency Nano-crystalline Soft Magnetic Materials, Institute for Materials Research, Tohoku University, Sendai 980-8577, Japan*
[2]*Institute for Materials Research, Tohoku University, Sendai 980-8577, Japan*

With the aim of applying to a magnetic core material, the effect of ribbon thickness on the magnetic properties of a (Fe, Co)-Si-B-P-Cu alloy ribbon was investigated. It is found that the Si addition in (Fe, Co)-Si-B-P-Cu nanocrystalline alloy increased the saturation magnetic flux density (B_s), but degraded the coercivity (H_c), suggesting that the Si addition should be suppressed to a little amount. It is also found that the replacement of Fe with Co is quite effective for obtaining better magnetic properties of Fe-Si-B-P-Cu alloy. Even for the thicker ribbons exceeding 30 μm in thickness, the nanocrystalline $Fe_{81.2}Co_4Si_{0.5}B_{9.5}P_4Cu_{0.8}$ alloy exhibited low H_c of 7 A/m and high B_s of 1.84 T. Such excellent magnetic properties were successfully reproduced in 50 mm wide ribbons. This regards that the nanocrystallized Co-containing alloy has high applicability to high-efficiency magnetic core material. [doi:10.2320/matertrans.MBW201402]

(Received September 16, 2014; Accepted November 10, 2014; Published December 19, 2014)

Keywords: *soft magnetic material, nanocrystalline alloy, high saturation magnetic flux density, low core loss*

1. Introduction

Soft magnetic alloys are used as a magnetic core material for various kinds of devices such as electrical power equipments and electronic appliances. In spite of unsatisfactory magnetic softness, silicon steel[1)] is still commercially used because of its high saturation magnetic flux density ($B_s \geq 1.90$ T), low material cost and good productivity. In such circumstances, new nanocrystalline soft magnetic alloys such as Fe-Si-B-Nb-Cu, FINEMET®[2,3)] and Fe-(Nb, Zr)-B, NANOPERM®[4)] with excellent magnetic softness have been developed in early 90's. Due to the relatively large content of high-cost elements such as Nb and Zr, as well as relatively lower B_s (1.2–1.7 T), practical applications of these nanocrystalline soft magnetic alloys have been limited. Hence, development of new soft magnetic alloys having both high B_s and good magnetic softness are still strongly required for miniaturization of high efficiency electrical devices.

Recently, nanocrystalline Fe-Si-B-P-Cu soft magnetic alloys, NANOMET® with high Fe content of above 83 at%[5–9)] have attracted much attention as a future core material for high performance magnetic applications because of their high B_s (≥1.80 T), low H_c, significantly low core loss (W) and low materials cost. Additionally, the Co addition to Fe-Si-B-P-Cu alloy is reported to be effective in improving the magnetic properties.[10)] The concentration of each element present in the alloy affects the structure, and magnetic properties.[8,11)] Therefore, it is necessary to optimize the alloy composition and understand the relationship between structure and magnetic properties. For most of the nanocrystalline alloys, studies were made on thinner and smaller ribbons (~5 mm in width and 18 μm in thickness).[5–11)] However, for commercial applications, it is necessary to optimize the composition, and evaluate the properties of wider and thicker ribbons. For instance, the thickness of most commercialized Metglas® or FINEMET® ribbons[12)] is about 18–25 μm. Out of a large number of soft magnetic nanocrystalline alloys reported, only few of them were commercialized even though they exhibit good soft magnetic properties. This is because the composition and properties optimized for small width ribbons are not the same as those for wide ribbons. Considering the provision of high quality NANOMET® ribbons for commercial applications, it is preferable that the wide ribbons (≥50 mm) exhibit good soft magnetic properties in thickness range of ~18–25 μm or more. Recently, we have noticed that the maximum thickness of having amorphous structure in as-quenched state is sensitive to Si content in the alloy. Additionally, replacement of Fe with Co is effective to obtain good soft magnetic properties in thicker ribbons. Therefore, in this paper, we intend to clarify the dependency of ribbon thickness on magnetic properties for (Fe, Co)-Si-B-P-Cu alloys with different Si and Co contents. Moreover, we also present the results on optimization of alloy composition, which allows us to produce wider ribbons for commercial applications in power transformers and motors.

2. Experimental Procedure

$Fe_{85.2}Si_xB_{10-x}P_4Cu_{0.8}$ alloy ($x = 0.5$ and 2 at%) and $Fe_{81.2}Co_4Si_{0.5}B_{9.5}P_4Cu_{0.8}$ alloy (replacement of Co for Fe to 0.5 at% Si-containing alloy) ingots were prepared by a high frequency induction melting of a mixture of Fe (99.9 mass%), Co (99.5 mass%), Si (99.999 mass%), B (99.5 mass%), Cu (99.99 mass%) and pre-melted Fe_3P (99 mass%) in Ar atmosphere. Rapidly solidified ribbons with a constant width of about 10 or 50 mm and different thicknesses of 15–33 μm were produced by a single roller melt-spinning method. The as-quenched ribbons were annealed at various temperatures for 600 s in flowing Ar atmosphere by using an infrared furnace equipment with a constant heating rate of 5°C/s. The structure of the as-quenched and annealed alloy ribbons was examined by an X-ray diffractometer (XRD) and a transmission electron microscopy (TEM). Thermal properties were evaluated using a differential scanning calorimeter

*Corresponding author, E-mail: k-takenaka@imr.tohoku.ac.jp

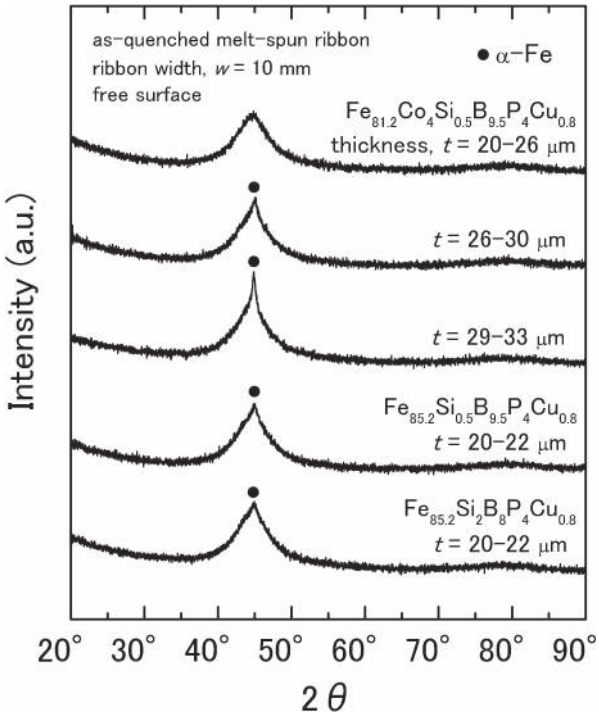

Fig. 1 XRD profiles of the as-quenched $Fe_{81.2}Co_4Si_{0.5}B_{9.5}P_4Cu_{0.8}$ alloy ribbons with a thicknesses of 20–26, 26–30 and 29–33 μm and the Co-free $Fe_{85.2}Si_{0.5}B_{9.5}P_4Cu_{0.8}$ and $Fe_{85.2}Si_2B_8P_4Cu_{0.8}$ alloy ribbons with a thickness of 20–22 μm.

(DSC) and a differential thermal analyzer (DTA) at heating rates of 0.67°C/s and 0.167°C/s, respectively, under Ar atmosphere. B_s and H_c of the nanocrystallized ribbons were measured using a vibrating sample magnetometer (VSM) and a DC B-H loop tracer with a solenoidal coil under a maximum applied field of 800 kA/m and 2–4 kA/m, respectively. The W at 50 Hz was measured by using an AC B-H analyzer.

3. Results and Discussion

The properties of nanocrystalline ribbons obtained after annealing is strongly influenced by the structure in as-quenched state. Figure 1 shows the XRD profiles taken from the free surface of the as-quenched $Fe_{81.2}Co_4Si_{0.5}B_{9.5}P_4Cu_{0.8}$ alloy ribbons with a constant width of 10 mm and different thicknesses of about 20–26, 26–30 and 29–33 μm. The data of the Co-free $Fe_{85.2}Si_{0.5}B_{9.5}P_4Cu_{0.8}$ and $Fe_{85.2}Si_2B_8P_4Cu_{0.8}$ alloy ribbons with a thickness of about 20–22 μm are also shown for comparison. For both the Co-free alloy ribbons with different Si content, even with a thickness of about 21 μm, a weak sharp Bragg peak superimposed on a broad diffraction peak at $2\theta = 45°$ is noticeable. This sharp peak in XRD was found to disappear after polishing of ribbon surface (not shown here). The presence of a weak sharp peak, and its absence after polishing suggest precipitation of α-Fe grains in the amorphous matrix, especially near the free surface. No significant difference in the amorphous-forming ability (AFA) caused by the variation of Si content could be found. On the other hand, for the Co-containing $Fe_{81.2}Co_4Si_{0.5}B_{9.5}P_4Cu_{0.8}$ ribbon, the profile taken from the thick ribbon with a thickness of 20–26 μm has only a broad diffraction peak, confirming only an amorphous phase. Liquidus temperature (T_l) of the Co-containing alloy was 1192°C which is about 40 degrees lower than that of the Co-free alloys ($T_l = \sim 1230$°C). It seems that the decrease in T_l facilitates the amorphous phase formation because it increases the cooling rate during ribbon preparation. Although the further increase in ribbon thickness leads to a precipitation of α-Fe, no drastic change in structure was detected for the thicker ribbons of thickness ~26–30 μm. The XRD measurements (not shown here) on as-quenched and surface polished ribbons confirmed that the crystallization is only at the ribbon surface. These XRD results suggest that partial replacement of Fe with Co in Fe-Si-B-P-Cu alloy increase the AFA of the alloy, and the critical thickness for the formation of single amorphous phase is about 26 μm for the $Fe_{81.2}Co_4Si_{0.5}B_{9.5}P_4Cu_{0.8}$ alloy and below 20 μm for the $Fe_{85.2}Si_{0.5}B_{9.5}P_4Cu_{0.8}$ and $Fe_{85.2}Si_2B_8P_4Cu_{0.8}$ alloys.

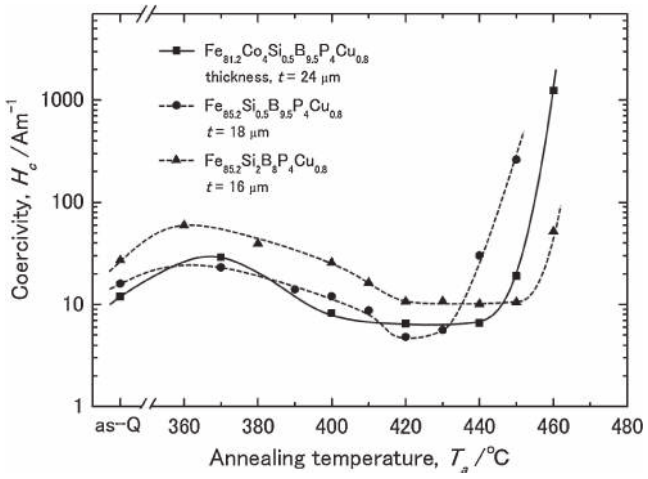

Fig. 2 Change in H_c value of the $Fe_{81.2}Co_4Si_{0.5}B_{9.5}P_4Cu_{0.8}$, $Fe_{85.2}Si_{0.5}B_{9.5}P_4Cu_{0.8}$ and $Fe_{85.2}Si_2B_8P_4Cu_{0.8}$ alloy ribbons as a function of T_a.

Before understanding the effects of ribbon thickness on magnetic properties, optimum annealing temperature for nanocrystallization of each alloy was investigated. Figure 2 shows the changes in H_c for $Fe_{81.2}Co_4Si_{0.5}B_{9.5}P_4Cu_{0.8}$, $Fe_{85.2}Si_{0.5}B_{9.5}P_4Cu_{0.8}$ and $Fe_{85.2}Si_2B_8P_4Cu_{0.8}$ ribbons as a function of annealing temperature (T_a). The annealing temperature sensitivity on magnetic properties is an important factor for the practical application of materials. The structure of 24, 18 and 16 μm thick ribbons is amorphous, which was confirmed by XRD measurements. The annealing at low temperature of $T_a = 360$–370°C leads to an increase in H_c. Above $T_a = 380$°C, H_c starts to decrease due to the precipitation of α-Fe grains in the amorphous matrix (the primary crystallization) and finally increases drastically by the rapid grain growth and precipitation of secondary compound phases other than α-Fe (the secondary crystallization).[5,7] The minimum H_c of each ribbon is evaluated to be 6.5 A/m at $T_a = 420$°C, 4.8 A/m at $T_a = 420$°C and 10 A/m at $T_a = 440$°C for the $Fe_{81.2}Co_4Si_{0.5}B_{9.5}P_4Cu_{0.8}$, $Fe_{85.2}Si_{0.5}B_{9.5}P_4Cu_{0.8}$ and $Fe_{85.2}Si_2B_8P_4Cu_{0.8}$ alloy ribbons, respectively. From the XRD profiles, their mean of α-Fe grain sizes evaluated by Scherrer's equation were 15, 14 and 18 nm, respectively. These results revealed that the structure of both the Co-free and Co containing alloys (with 0.5 at%

Si) is made from nano-sized α-Fe grains. The low H_c is due to a finer nano-crystalline structure, which results in the averaging of magneto-crystalline anisotropy by strong magnetic exchange coupling among the α-Fe grains. On the other hand, a large difference in annealing temperature sensitivity on H_c was found among the alloy compositions. Low H_c of less than 10 A/m for the $Fe_{81.2}Co_4Si_{0.5}B_{9.5}P_4Cu_{0.8}$, $Fe_{85.2}Si_{0.5}B_{9.5}P_4Cu_{0.8}$ and $Fe_{85.2}Si_2B_8P_4Cu_{0.8}$ ribbons was obtained in the T_a range of 400–440°C, 410–430°C and 420–450°C, respectively. Thermal analysis by DSC (Fig. 3) shows that the primary crystallization temperatures (T_{x1}) for all the alloys are almost the same ranging from 389–393°C, but the secondary crystallization temperatures (T_{x2}) are different depending on the alloy composition. The minimum

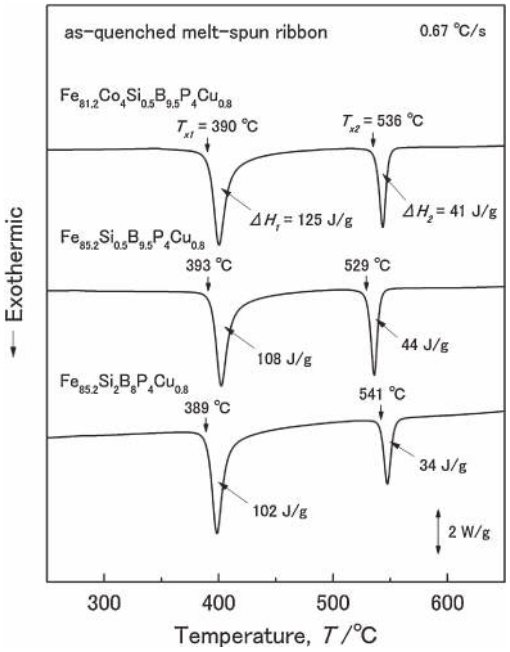

Fig. 3 DSC curves of the $Fe_{81.2}Co_4Si_{0.5}B_{9.5}P_4Cu_{0.8}$, $Fe_{85.2}Si_{0.5}B_{9.5}P_4Cu_{0.8}$ and $Fe_{85.2}Si_2B_8P_4Cu_{0.8}$ alloy ribbons.

T_a for obtaining the lowest H_c is low for the Co-containing alloy compared to that of the Co-free alloy. Additionally the T_a range for having a low H_c is wider for Co-containing alloy, which means the nano-strcture is relatively stable. For both the 0.5 at% Si-containing alloys, an exothermic heat induced by the precipitation of α-Fe grains (ΔH_1) in the Co-free alloy was nearly 15% smaller than that of the Co-containing alloy. The ΔH_1 depends on the ribbon thickness and the production conditions. A minor crystallization in as-quenched state can reduce the ΔH_1. Therefore, a situation can exist, where both the Co-free and Co-containing alloys may have similar ΔH_1. However, for as-quenched amorphous ribbons, the ΔH_1 can be related to the crystallization fraction, which means higher the ΔH_1, larger is the formation of α-Fe. In the present alloys, the crystallization fraction of α-Fe depends on the total number of nuclei, which are the sum of pre-existing (i.e. as-quenched) and the newly formed nuclei of α-Fe on annealing.[13] We have noticed that the relative heat released in primary crystallization [i.e. $\Delta H_1/(\Delta H_1 + \Delta H_2)$; ΔH_2, is the area of second peak in DSC curve] is higher (~75%) for 0.5 at% Si in Co-containing alloy compared to Co-free one (~71%). It seems the number of α-Fe nuclei are larger in the case of Co-containing alloy. The number of pre-existing nuclei depends on as the as-quenched state of the ribbon. A small difference in the as-quenched structure may influence the minimum T_a required for obtaining a low H_c. Additionally a larger number of nuclei can make the nanostructure more stable and uniform.[13] A constant H_c in a wide annealing temperature range for the Co-added alloy in Fig. 2 is a clear evidence for stable nano-structure. This characteristic insensitivity to T_a means the better controllability in mass production. From these results, magnetic property evaluations for ribbons with different thickness were carried out using the ribbons with lowest H_c obtained by optimal annealing conditions.

Figure 4 shows the variations in H_c and B_s as a function of ribbon thickness for the $Fe_{81.2}Co_4Si_{0.5}B_{9.5}P_4Cu_{0.8}$, $Fe_{85.2}Si_{0.5}B_{9.5}P_4Cu_{0.8}$ and $Fe_{85.2}Si_2B_8P_4Cu_{0.8}$ alloy ribbons after nanocrystallization at $T_a = 420$°C, 420°C and 440°C, respec-

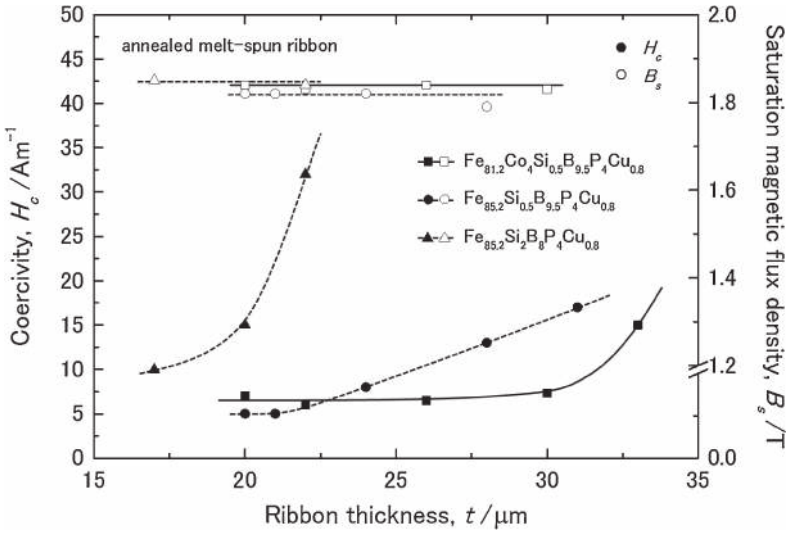

Fig. 4 Change in H_c and B_s for the nanocrystalline $Fe_{81.2}Co_4Si_{0.5}B_{9.5}P_4Cu_{0.8}$, $Fe_{85.2}Si_{0.5}B_{9.5}P_4Cu_{0.8}$ and $Fe_{85.2}Si_2B_8P_4Cu_{0.8}$ alloy as a function of ribbon thickness.

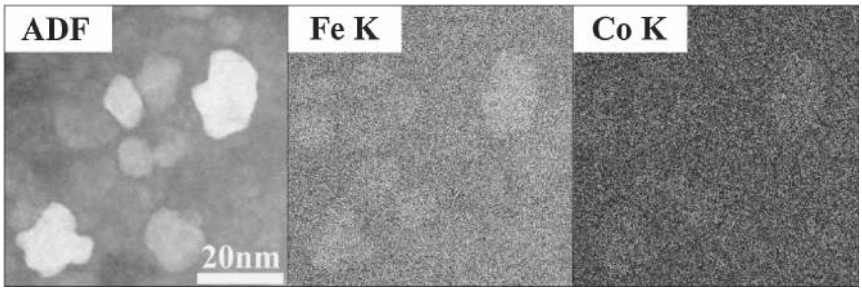

Fig. 5 ADF image, Fe and Co K-line intensity maps for the nanocrystallized Co-containing alloy ribbon.

tively. A significant difference in their dependence of ribbon thickness on H_c for Co-free alloys can be found. The H_c of 2 at% Si-containing alloy drastically increases with increasing ribbon thickness for the thickness higher than 20 μm, the 0.5 at% Si-containing ribbon exhibits low H_c of less than 10 A/m for the thickness of 20–24 μm. For the 0.5 at% Si-containing alloy, the critical thickness (t_{cri}) for obtaining low H_c of less than 10 A/m was evaluated to be 24 μm and the H_c gradually increased as ribbon got thicker. In spite of no distinct difference in as-quenched structure for both ribbons with about 21 μm in thickness (see Fig. 1), it was found that H_c characteristics change depending on Si-content. These results suggest that the alloy containing small amount of Si is preferred to produce thicker ribbon with low H_c. However, slightly low B_s was confirmed in the 0.5 at% Si-containing alloy. The B_s of 0.5 and 2 at% Si-containing alloy ribbons without Co was evaluated to be 1.82 and 1.85 T, respectively, and found to be independent on ribbon thickness. From DSC measurements (see Fig. 3), the exothermic heat induced by a precipitation of secondary crystalline phases except α-Fe grains (ΔH_2) in the 2 at% Si-containing alloy was about 20% smaller than that of the 0.5 at% Si-containing one. Alternatively, the relative heat released $[\Delta H_1/(\Delta H_1 + \Delta H_2)]$ in primary crystallization of 2 at% Si-containing alloy (∼75%) is larger than the 0.5 at% Si alloy (∼71%). The results suggest that the 2 at% Si-containing alloy contains a larger volume fraction of α-Fe grains, leading to higher B_s. Moreover, the t_{cri} is less than 25 μm for both the Co-free alloys, which restricts their application field (except for high-frequency application). On the other hand, the t_{cri} remarkably improved by the Co addition. The ribbon of 30 μm in thickness exhibits low H_c of 7.3 A/m, which is almost the same as that of the ribbon of 20 μm in thickness ($H_c = 7.0$ A/m). Although the precipitation of α-Fe grains near the free surface was confirmed by XRD measurement for the thick ribbon in as-quenched state (see Fig. 1), it seems that there are no coarse grains leading to degradation of H_c as seen in thick Co-free alloy ribbons. The average grain size of 30 μm thick Co-containing ribbon was 16 nm, and no precipitation of secondary phases was detected in the XRD pattern. In addition, it was confirmed that B_s increases by the Co addition and was evaluated to be 1.84 T, which is slightly higher than that of the Co-free alloy even with the same contents of metalloid elements ($B_s = 1.82$ T). Figure 5 shows the annular dark field (ADF) image, Fe and Co K-line intensity maps for the nanocrystallized Co-containing alloy ribbon. The elemental contrast for Fe and Co is present throughout the analyzed area. The reason for it may be the signal originating from the α-Fe grains present beneath the intergranular layer. However, a careful examination of the maps revealed a slightly higher contrast in the region of crystalline grains. This suggests that the Co and Fe are enriched in the grains i.e. Co atoms are present in the α-Fe grains. We believe the improved B_s by the Co addition is due to the solid solute effect of Co atom in α-Fe grain (see Slater-Pauling curve[14]). In addition to it, a relatively larger volume fraction of α-Fe is also contributing for the increase in B_s. From these results, it was found that the excellent properties possible for electrical device application are obtained by the Co-added Fe-Si-B-P-Cu alloy with low Si content. The B_s, H_c and t_{cri} of the present Co-containing alloy ribbon were evaluated to be 1.84 T, 7 A/m and about 30 μm, respectively. The t_{cri} is the same as or thicker than the thickness of most commercialized alloy ribbons and meets the thickness requirement for application.

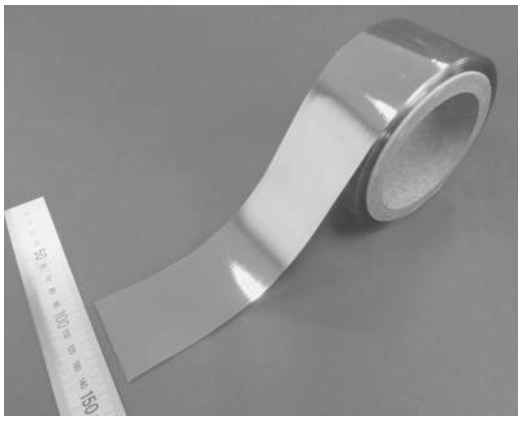

Fig. 6 Outer appearance of wide ribbon with 50 mm in width.

The above-mentioned results mean that the best properties (i.e. significantly low H_c, sufficiently high B_s and thick t_{cri}) are achieved by the nanocrystalline $Fe_{81.2}Co_4Si_{0.5}B_{9.5}P_4Cu_{0.8}$ alloy (that is, the low Si content Co-containing alloy). For applications, wide ribbons with a width of at least 20 mm are required. Hence, we have made investigations on the preparation and properties $Fe_{81.2}Co_4Si_{0.5}B_{9.5}P_4Cu_{0.8}$ alloy ribbons with 50 mm in width. Figure 6 shows the outer shape and surface appearance of wide ribbon with 50 mm in width. A melt-spun amorphous ribbon with 50 mm in width, ∼65 m in length, and ∼25 μm in thickness was made easily in air. It was confirmed that the H_c and B_s of the nanocrystallized ribbon annealed at $T_a = 420$°C are 7.0 A/m and 1.84 T, respectively, which are very close to the ribbons of 10 mm in

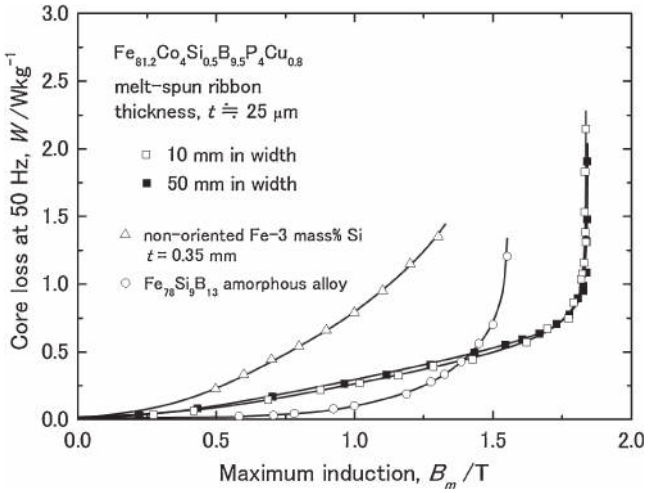

Fig. 7 W at 50 Hz of the nanocrystalline $Fe_{81.2}Co_4Si_{0.5}B_{9.5}P_4Cu_{0.8}$ alloy wide ribbon as a function of B_m.

width. The independence of magnetic properties on the ribbon width is a pre-requisite for practical applications.

In order to apply these ribbons in magnetic core applications, in addition to H_c and B_s, core-loss (W) characteristics are also important. Figure 7 shows the W at 50 Hz for the 50 mm wide nanocrystalline $Fe_{81.2}Co_4Si_{0.5}B_{9.5}P_4Cu_{0.8}$ alloy ribbon as a function of maximum magnetic flux density (B_m). The data of the ribbon with 10 mm in width and 25 μm in thickness having the same alloy composition, the commercially-used non-oriented magnetic steel[15] and Fe-based $Fe_{78}Si_9B_{13}$ amorphous alloy ribbon (Metglas®)[16] are also shown for comparison. The present nanocrystalline alloy exhibited W characteristics independent on the ribbon width. The W under B_m of 1.5 and 1.7 T was evaluated to be 0.52 and 0.66 W/kg, respectively for the 50 mm-wide ribbon and 0.44 and 0.66 W/kg, respectively for the 10 mm-wide ribbon. These properties are almost the same as those of previous-reported Fe-Si-B-P-Cu alloy,[5,7–11] except that the present ribbon sample is much thicker. As compared with the commercial alloys, the present nanocrystalline alloy ribbons showed much lower W at B_m of especially above about 1.5 T. It is therefore concluded that the nanocrystalline $Fe_{81.2}Co_4Si_{0.5}B_{9.5}P_4Cu_{0.8}$ alloy with excellent soft magnetic properties can be fabricated into thick and wide ribbon, which is required for practical use. This regards this alloy as one of the promising candidates for a high-efficiency magnetic core materials.

4. Conclusions

The dependence of ribbon width and thickness on magnetic properties for (Fe, Co)-Si-B-P-Cu alloys with different Si and Co contents was investigated. The conclusions are summarized as follows.

(1) For the Co-free alloys, increasing Si content is effective for obtaining high B_s. However, it leads to difficulties in obtaining low H_c of less than 10 A/m for thick-ribbons.
(2) Co addition is effective to enhance AFA and obtain high B_s in the annealed state. The nanocrystalline $Fe_{81.2}Co_4Si_{0.5}B_{9.5}P_4Cu_{0.8}$ alloy exhibits low H_c of 7 A/m and high B_s of 1.84 T; the properties remains unchanged even for the thick ribbon of 30 μm in thickness.
(3) Wide ribbon with a width of 50 mm and a thickness of about 25 μm of $Fe_{81.2}Co_4Si_{0.5}B_{9.5}P_4Cu_{0.8}$ alloy was successfully produced. Its excellent soft magnetic properties are independent of ribbon width up to 50 mm. These results suggest that the nanocrystalline alloy is a promising material for a high-efficiency magnetic core.

Acknowledgement

This work was supported by "Tohoku Innovative Materials Technology Initiatives for Reconstruction (TIMT)" funded by the Ministry of Education, Culture, Sports, Science and Technology (MEXT) and Reconstruction Agency, Japan. The authors are grateful to Dr. M. Nishijima for TEM observation.

REFERENCES

1) N. P. Goss: Trans. Am. Soc. Met. **23** (1935) 511–531.
2) Y. Yoshizawa, S. Oguma and K. Yamauchi: J. Appl. Phys. **64** (1988) 6044–6046.
3) Y. Yoshizawa and K. Yamauchi: J. Japan Inst. Metals **53** (1989) 241–248.
4) K. Suzuki, A. Makino, N. Kataoka, A. Inoue and T. Masumoto: Mater. Trans., JIM **32** (1991) 93–102.
5) A. Makino, H. Men, T. Kubota, K. Yubuta and A. Inoue: Mater. Trans. **50** (2009) 204–209.
6) F. Kong, A. Wang, X. Fan, H. Men, B. L. Shen, G. Xie, A. Makino and A. Inoue: J. Appl. Phys. **109** (2011) 07A303.
7) Z. Zhang, P. Sharma and A. Makino: J. Appl. Phys. **112** (2012) 103902.
8) A. Makino: IEEE Trans. Magn. **48** (2012) 1331–1335.
9) F. Kong, H. Men, T. Liu and B. L. Shen: J. Appl. Phys. **111** (2012) 07A311.
10) Y. Zhang, P. Sharma and A. Makino: IEEE Trans. Magn. **50** (2014) 2003004.
11) K. Takenaka, M. Nishijima and A. Makino: IEEE Trans. Magn. **50** (2014) 2004704.
12) https://www.hitachi-metals.co.jp/e/products/elec/tel/pdf/hl-fm9-e.pdf
13) P. Sharma, X. Zhang, Y. Zhang and A. Makino: Scr. Mater. (2014) http://dx.doi.org/10.1016/j.scriptamat.2014.08.023
14) C. Kuhrt and L. Schultz: J. Appl. Phys. **73** (1993) 6588–6590.
15) http://www.nssmc.com/en/product/sheet/index.html
16) http://www.metglas.com/products/magnetic_materials/